Optimized thermal coupling of micro thermoelectric generators for improved output performance

N. Wojtas [a],[*], L. Rüthemann [a], W. Glatz [b], C. Hierold [a]

[a] Micro and Nanosystems, ETH Zurich, Tannenstrasse 3, 8092 Zurich, Switzerland
[b] greenTEG GmbH, Technoparkstrasse 1, 8005 Zurich, Switzerland

ABSTRACT

There is a significant push to increase the output power of thermoelectric generators (TEGs) in order to make them more competitive energy harvesters. The thermal coupling of TEGs has a major impact on the effective temperature gradient across the generator and therefore the power output achieved. The application of micro fluidic heat transfer systems (µHTS) can significantly reduce the thermal contact resistance and thus enhance the TEG's performance. This paper reports on the characterization and optimization of a µTEG integrated with a two layer µHTS. The main advantage of the presented system is the combination of very low heat transfer resistances with small pumping powers in a compact volume. The influence of the most relevant system parameters, i.e. microchannel width, applied flow rate and the µTEG thickness on the system's net output performance are investigated. The dimensions of the µHTS/ µTEG system can be optimized for specific temperature application ranges, and the maximum net power can be tracked by adjusting the heat transfer resistance during operation. A system net output power of 126 mW/cm^2 was achieved with a module ZT of 0.1 at a fluid flow rate of 0.07 l/min and an applied temperature difference of 95K.

It was concluded that for systems with good thermal coupling, the thermoelectric material optimization should focus more on the power factor than on the figure of merit ZT itself, since the influence of the thermal resistance of the TE material is negligible.

© 2013 Elsevier Ltd. All rights reserved.

1. Introduction

Due to the simultaneous rise in energy consumption and environmental awareness, the worldwide demand for more efficient and clean energy systems is growing. One promising approach to improve a system's efficiency is to recover the produced waste heat by means of the thermoelectric effect. Thermoelectric power generation can potentially be applied for waste heat recovery in energy conversion systems [1], industrial processes [2] or automotive applications [2,3]. So far, however, the commercial applications of thermoelectric generators (TEGs) have been limited to niche markets, such as space [4,5] and remote or hazardous places [6,7]. The main reasons for this are (1) the relatively low thermoelectric conversion efficiency, (2) high fabrication costs of thermoelectric modules, and (3) suboptimal exploitation of the available temperature

gradients. While much effort is spent to improve the thermoelectric figure of merit (ZT) by quantum confinement or phonon scattering [8–10] as well as to develop low-cost fabrication technologies [11], less attention has been paid to the optimization of the overall system's performance so far. This includes thermal coupling of the thermoelectric device to the heat source and heat sink, as well as an optimal matching of the thermal contact and TEG resistances [12]. By decreasing the thermal contact resistance to the cold and hot side reservoir, a significant enhancement of the generator's output power can be achieved [13]. The major impact of the thermal contact resistance on the output performance of a thermoelectric generator is illustrated in Fig. 1 and compared to the effect of ZT. While the influence of ZT on the output power has a close to linear dependency, the thermal contact resistance exhibits a power dependency proportional to $1/R_{Con}^2$.

The most straight-forward approach to achieve small thermal contact resistances is to apply fluidic heat exchanger systems for the heat supply and dissipation. This is also the most effective method for waste heat recovery. Several large scale fluidic systems using liquid as active media have been tested for use in industrial applications. Tsuyoshi et al. [14] reported experimental results on a

* Corresponding author. ETH Zurich, Micro and Nanosystems, CLA J11.1, Tannenstrasse 3, 8092 Zurich, Switzerland. Tel.: +41 44 632 48 99; fax: +41 44 632 14 62.
E-mail addresses: nwojtas@ethz.ch, wojtas@micro.mavt.ethz.ch (N. Wojtas).
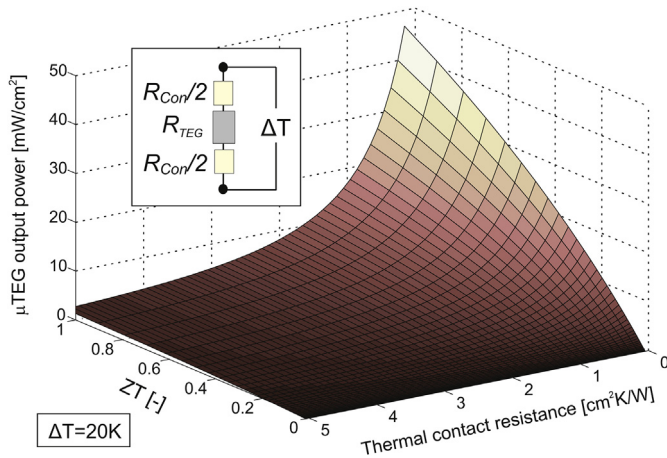
Fig. 1. Simulated output power of a 215 μm thick Bi_2Te_3 μTEG (R_{TEG} = 2.8 cm^{2}K/W) in dependence of the ZT-value and the thermal contact resistance R_{Con} at an applied temperature difference of 20K. The simulations were performed applying a thermo-electric model under matched electrical load [17].

Fig. 2. Exploded view of the μHTS/μTEG system.

thermoelectric engine made out of TEGs stacked between a parallel plate heat exchanger using oil and water as active media. At an applied temperature gradient of 130K, an output power of 170 W could be reached. Niu et al. [15] built a similar parallel plate heat exchanger with commercially available Bi_2Te_3 modules reaching, 140 W at an inlet temperature difference of 120K. Crane et al. [2] constructed a TEG-heat exchange assembly with a stack of 6 TEG modules producing 500 W at an inlet temperature difference of 205K. Due to the growing interest in thermoelectric waste heat recovery for automotive applications, several gas/liquid heat exchange systems have been studied and tested [3]. First functional prototypes have already been installed in test engines and values as high as 507 W at a ΔT of 553K could be reached [16].

Although the achieved output power values from the experimental studies are remarkable, the systems are generally very large and heavy resulting in rather low output powers per volume. Often, standard large scale heat exchangers are applied, where high amounts of the working fluid are pumped through the system and the consumed pumping power is neglected. Furthermore, the reported systems usually work without optimized thermal contact resistance and overall system performance. In contrast, scaling down the heat exchangers to the micrometer range brings several advantages. Micro heat transfer systems (μHTS) can achieve high heat fluxes due to an increase of the convective heat transfer coefficient as well as of the surface area [17]. Even though μHTS generally exhibit larger hydrodynamic resistances, the effect on the pumping power can be compensated by smart design and smaller flow rates needed. With the reduced heat transfer resistances, thinner generators can be applied for thermal resistance matching. This makes the system compatible for waste heat recovery in industrial applications, where high heat fluxes are often necessary. Additionally, more compact systems with reduced size and weight can be built, resulting in increased applicability and modularity of the system. The performance characteristic of different micro heat sinks for chip or LED cooling applications have been investigated in several theoretical and experimental studies [17,18]. Rezania et al. [19] evaluated the theoretical performance of a thermoelectric generator using a rectangular microchannel heat sink. The simulation results showed no net TEG power improvements of the micro heat sink system compared to macro scale heat sinks, mainly due to the large pressure drops inside the microchannels. To avoid such large pressure losses and to still benefit from the improved thermal performance of microchannels, multiple layer manifold systems can be applied [20–22].
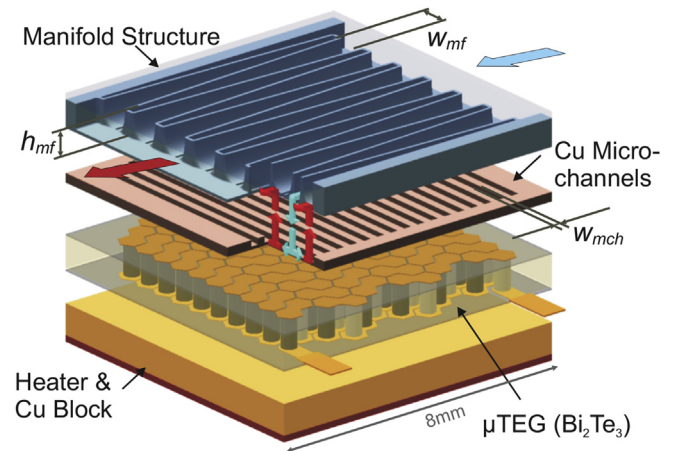
Therefore, a novel approach of minimizing thermal resistances by integrating two layer μHTS with μTEGs is proposed. This paper presents an experimental study on the performance of such an integrated system as shown in Fig. 2. The μHTS consists of a copper microchannel layer for efficient heat removal and a polymeric manifold channel layer responsible for the fluid distribution [13]. Besides a small pressure loss and a low heat transfer resistance, the proposed system also benefits from uniform cooling properties. Many different sets of parameters influence the performance of the described μHTS/μTEG system; namely the dimensions of the μHTS itself, the properties and dimensions of the thermoelectric generator and the applied boundary or working conditions. The paper focuses on the analysis and characterization of the most important μHTS/μTEG system parameters with the aim of optimizing the overall system's net output performance. In the first part, the μHTS is characterized in regards to the system's dimensions, flow rates and applied temperature gradients. In the second part, the output power of the μHTS/μTEG systems is investigated with respect to the μHTS dimensions, boundary conditions and μTEG thermal properties. The advantages of variable thermal resistances are discussed, and practical aspects of the thermal resistance matching are evaluated.

2. Experimental

The μHTSs were designed based on system and fabrication constraints in combination with performed simulations results. The parameter with the largest impact on the thermal and hydrodynamic performance of the μHTS was identified to be the microchannel dimensions. Therefore, μHTSs with different channel widths were fabricated and analyzed. The relevant parameters of the μHTSs used are summarized the Table 1.

The investigated μHTSs were fabricated using standard photolithography and electrochemical deposition. The detailed working principle and the fabrication process of the μHTS are reported in Ref. [13]. The μTEGs used were provided by greenTEG GmbH and are based on the electrodeposition of Bi_2Te_3 thermoelectric material into flexible polymer molds. A detailed fabrication process is

Table 1
μHTS design parameters.

Microchannel width − w_{mch} [μm]	Microchannel height − h_{mch} [μm]	Fin/channel ratio [−]	Manifold channels width − w_{mf} [μm]	Manifold channels height − h_{mf} [μm]	Total area [mm]
35, 50, 60, 80	190	1	150−300 (tapered)	1000	8 × 8

described in Ref. [11]. In order to provide electrical isolation, a 2.5 μm layer of photoresist (Microposit S1813, Shipley) was deposited as a passivation layer on each side of the μTEG. To minimize the interface resistance to the μHTS and the heater, the passivated generator was additionally covered with approximately 30−40 μm thermal paste (Dow Corning TC-5026). Prior to their integration into the μHTS, the μTEG-units were characterized in a thermoelectric measurement setup [23]. The relevant parameters of the standard μTEG used are summarized the Table 2. The module ZT is defined as the figure of merit of the generator, where the complete μTEG resistance (including electric contact resistance and the interconnect resistance) is used for the electric resistivity calculation.

For the characterization of μHTSs and μHTS/μTEG systems, the devices were mounted on a clamping fixture and connected to a controlled fluid loop [13]. The clamped μHTS/μTEG system and its equivalent thermal circuit model are schematically depicted in Fig. 3. The measurement fixture contains a resistive heater (platinum meander on Al_2O_3 substrate), a copper block with an integrated temperature sensor and a pressure controlled clamping tool. The equivalent thermal circuit of the μHTS/μTEG systems consists of the heat transfer resistance of the μHTS R_{HTS}, the thermal resistance of the generator R_{TEG} and the interface resistances $R_{Interface}$ accounting for the electrical passivation layer of the TEG and the thermal paste. Therefore, the total contact resistance is defined as the sum of the variable R_{HTS}, and the two $R_{Interface}$.

The cooling liquid (DI water) flow was measured by means of a Coriolis flow meter (error: ±1% of reading). The pressure drop across the μHTS was recorded with a differential pressure sensor (error: ±1 mbar). The consumed pumping power was calculated from the product of the fluid flow and the measured pressure drop. The heat flux through the system was defined by the power consumed by the temperature controlled heater. The heat transfer resistance of the μHTS was calculated by dividing the applied temperature difference ΔT by the measured heat flux. The thermoelectric power output was calculated from the measured Seebeck voltage V_{SB} under electrically matched loads conditions and corresponds to the maximal achievable power output [24]. A fluid inlet temperature of 293K, a tool pressure of 660 kPa, a measurement duration of 120 s and a sampling frequency of 0.76 s^{-1} were defined as standard test conditions.

Before the performance measurements of the μHTS/μTEGs systems, the μHTSs were characterized with respect to their thermal and hydrodynamic performance inside the fluid loop measurement setup. To investigate optimal system dimensions, μHTSs with four different microchannel widths were analyzed (Table 1). Additionally, the influence of external boundary conditions on the μHTS performance, i.e. the fluid inlet temperature and heater temperature, was studied. The net output performance of the μHTS/μTEG system was characterized with respect to the fluid flow rate, the applied temperature gradient and the microchannel dimensions. The influence of thermal resistance matching by μTEG thickness variations was also investigated. For this purpose, the μTEG was ground down to three different heights and re-contacted after each grinding step.

The measurement uncertainty was calculated according to ISO/IEC 17025 standards [25]. The resulting standard deviation from the
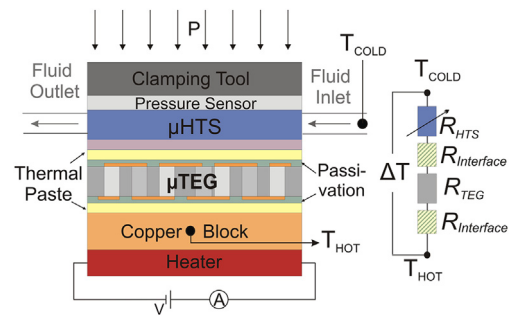

Fig. 3. Schematic of the μHTS/μTEG system clamped inside the measurement fixture and its equivalent thermal circuit model.

time averaged measurement signals (random error) was combined with measurement equipment errors (systematic errors). The Gauss propagation of uncertainty was used for error calculations of indirectly measured values (R_{HTS}, P_{Pump}, P_{TEG}). The measurement repeatability of the clamping structure was tested by multiple mountings of the same μHTSs and μHTS/μTEG devices. The maximum measured standard deviation errors were below 5.3% and 0.52% for the measured heat transfer resistance R_{HTS} and Seebeck voltage V_{SB}, respectively. This measured standard deviations of the clamping influence are all below the calculated measurement uncertainty plotted as error bars in the figures.

The μHTS model used was a semi-empirical one-dimensional model [26] extended with a discrete temperature distribution along the fluid path inside the microchannels and temperature dependent fluid parameters. The modeled R_{HTS} is composed of three thermal resistances in series: the conductive resistance through the microchannels, the convective resistance at the fluid−channel interface and the fluid resistance due to the limited heat capacity. The resistance of the thermal paste was fitted to 0.08 cm^{2}K/W corresponding to a layer thickness of 30 μm. For flows below 0.4 l/min, a correction factor was introduced in order to account for a reduced heat transfer due to randomly trapped air bubbles in the microchannels and possible heating up of the fluid inside the manifold channels. For the μHTS/μTEG system, the 1D model was extended with a TEG model under matched electrical load, taking Joule heating and Peltier effects into account [27]. Interface resistances accounting for the electrical passivation and the thermally conductive paste were added (0.22 cm^{2}K/W at each side). The measured μTEG and μHTS parameters from Tables 1 and 2 were used for the simulations.

3. Results and discussion

3.1. μHTS characterization

The thermal and hydrodynamic performance of the μHTS with different microchannel dimensions was investigated, and the influences of varying boundary conditions were analyzed. Fig. 4a) shows the measured and computed heat transfer resistance R_{HTS} of the μHTSs with different microchannel dimensions relative to the fluid flow rate. The heat transfer resistance decreases with increasing flow rates mostly due to a rise in the heat capacity rate of the fluid. The curves flatten down towards higher flow rates, since the relative influence of an increased effective mass flow on the heat flux is reduced. With decreasing channel widths, R_{HTS} is reduced mainly due to an increase in the convective heat transfer. At smaller microchannel widths, the thermal boundary layer is thinner and therefore the heat convection inside the channel is improved. Additionally, the effective heat transfer area per chip is increased. With the smallest channel size of 35 μm, a minimal heat transfer resistance of

Table 2
Measured Bi_2Te_3 μTEG parameters.

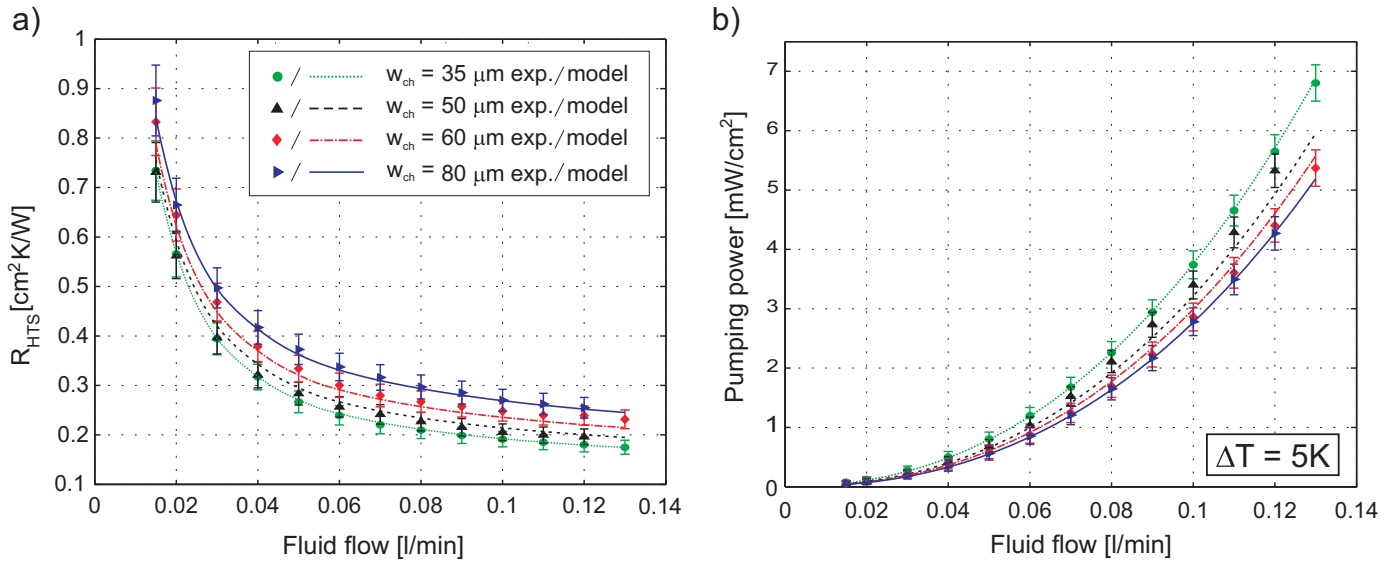| Module ZT [−]	Electrical resistance R_{El} [Ω]	Thermal resistance R_{TEG} [cm²K/W]	Total thickness [μm]	Ratio passive/TE material [−]
0.06 ± 0.01	2.35 ± 1E-3	5.1 ± 0.3	215 ± 10	1.43 ± 0.1

Fig. 4. Measured (markers) and computed (lines) performance of μHTSs with different microchannel widths as a function of the fluid flow rate at an applied ΔT of 5K: a) heat transfer resistance R_{HTS} and b) pumping power.

0.175 cm²K/W could be reached at a fluid flow of 0.13 l/min. The measured R_{HTS} also includes the resistance of the thermal paste located between the μHTS and the Cu heater (approx. 0.08 cm²K/W).

The power necessary to pump the fluid through the μHTS is depicted in Fig. 4b). The pumping power increases with larger fluid flows and smaller microchannel dimensions. The first is a result of an increased hydrodynamic resistance due to the increased flow velocity. The second can be explained by the higher shear forces (i.e. pressure losses) induced by a larger surface to volume ratio.

The experimental results are in good agreement with the simulation results. The heat transfer resistance (Fig. 4a)) shows two minor deviations from the computed values. First, the measured values are partly shifted upwards or downwards. Second, the slope at smaller fluid flows does not always correspond to the theory, resulting in a slight overestimation of the thermal performance. The first deviation mainly results from slightly different thicknesses of the thermal paste layer, since the exact thickness is very hard to control. The second deviation is likely related to the observed small air bubbles that can get trapped inside the microchannels at smaller fluid flows. This might clog some channels and thus reduce the heat convection. Although a correction factor was introduced to account for this phenomenon, its impact is random and can vary between samples and measurements. The deviation of the pumping power from the computed values (Fig. 4b)) can be explained by the limited fabrication accuracy of the device. Especially the connecting slots between the top manifold layer and bottom microchannels are likely sources of geometric deviations, due to the bonding and slot release processes [13].

In order to quantify the influence of the boundary conditions on the thermal and hydrodynamic properties of the μHTS, the fluid inlet temperature and the heater temperature were varied as well. By increasing the fluid temperature, an improvement of the overall system performance was observed. As a result of an inlet temperature increase of 2K ($T_{IN} = 295K$), the R_{HTS} measured at a fluid flow of 0.04 l/min decreases by 6% and the pumping power by 7% (averaged over 3 different samples). The reduction in R_{HTS} originates from the increase of the thermal conductivity of the fluid, resulting in an increased thermal convection at the microchannel walls and thus reduced convective resistance. The higher inlet temperatures of the fluid also reduce the mean fluid density and mean fluid kinetic viscosity. This decreases the hydrodynamic

resistance, leading to a smaller pressure drop and consequently smaller pumping powers.

The same trend is observed when the heater temperature is increased. However, the effect is less pronounced, since the fluid is heated up indirectly. In this case, an average improvement of 1% of the heat transfer resistance and 6% of P_{PUMP} was measured for a heater temperature increase by 10K ($T_{HOT} = 308K$) and a fluid flow of 0.04 l/min (averaged over 3 different samples). The measurement results demonstrate an improved thermal and hydrodynamic μHTS performance at higher operation temperatures. However, in the small investigated temperature ranges, the influence on the μHTS parameters is rather limited. Additionally, due to the measurement uncertainties, the given changes should be regarded as qualitative trends.

3.2. μTEG/μHTS performance

In order to evaluate the optimal μHTS/μTEG system performance, the influence of the working conditions (i.e. the applied thermal gradients), the microchannel dimensions and the μTEG thickness (i.e. thermal resistance) on the system's power output were investigated.

3.2.1. Influence of working conditions

Fig. 5a) shows the measured Seebeck voltage and the output power of the μTEG/μHTS system with respect to the applied temperature gradient and different fluid flow rates. In Fig. 5b), the corresponding net output power is depicted. The slope of the Seebeck voltage (dashed line) increases with increasing flow rates, i.e. decreasing heat transfer resistance R_{HTS}, due to an increased heat flux and therefore larger actual temperature gradient across the generator. However, the differences in the slopes are rather small due to a large μTEG thermal resistance R_{TEG} compared to the R_{HTS} variations, thus resulting in a relatively small influence of the enhanced heat transfer. The specific influence of the R_{TEG} to R_{HTS} ratio will be discussed in more detail in Section 3.2.3. Correspondingly, the differences in the μTEG output power (solid lines) shows only small deviations between different flow rates.

If the consumed pumping power is subtracted from the output power (Fig. 5b)), the influence of the flow rates increases significantly. Larger flows, consuming higher pumping powers, need
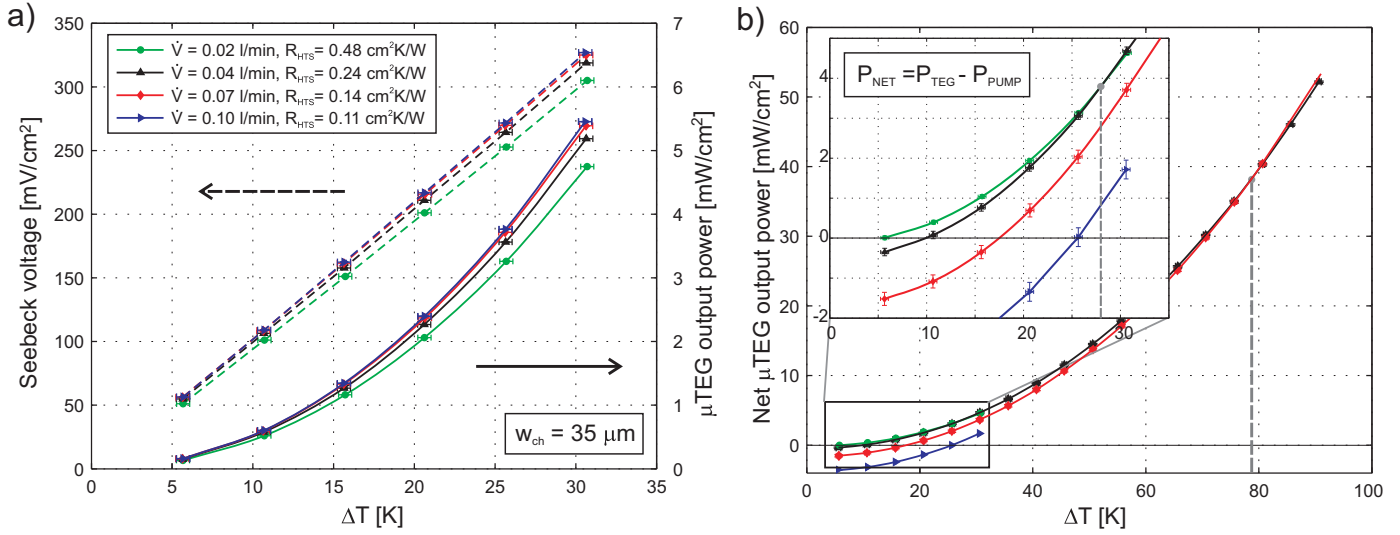
Fig. 5. a) Seebeck voltage (dashed lines) and output power (solid lines) measurements on the μHTS/μTEG system and b) net output power as a function of the applied ΔT and the fluid flow rate at w_{ch} = 35 μm.

higher temperature gradients to achieve a positive net output power. However, their slopes are steeper and therefore, at larger applied ΔT, higher flow rates outperform lower ones. The transition points for this system are marked in the graph by vertical dashed lines. This means that the system performance can be adapted to different operating conditions by varying the fluid flow rate. For operating conditions with small temperature gradients, small flow rates, i.e. large heat transfer resistances and small pumping powers, are advantageous. With increasing temperature gradients, the flow must be increased in order to track the maximal net output power of the system.

Fig. 6 shows the net output power for μTEGs with different ZT values as a function of the applied temperature gradient. At the maximal applied temperature difference of 95K, a net output power of 126.3 ± 1.5 mW/cm^2 was measured with a module $ZT = 0.1$ of the μTEG, resulting in an overall system thermoelectric efficiency factor of 14 μW/K^{2}cm^2. To show the performance potential of devices with improved thermoelectric material properties, a computed net power for a module $ZT = 1$ is added to the graph.
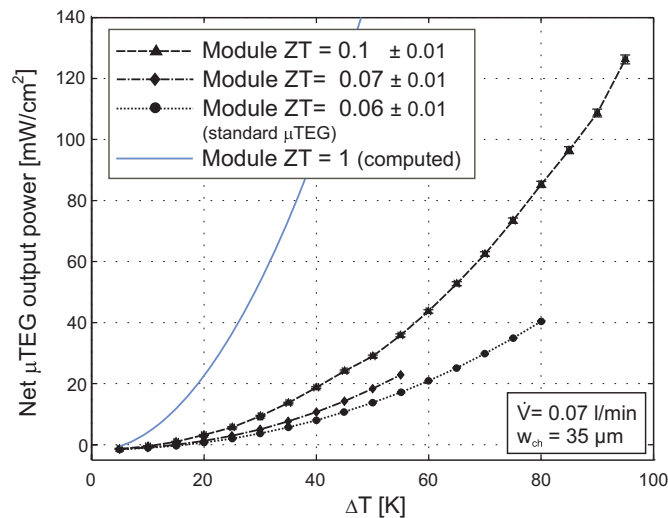
3.2.2. Influence of microchannel dimensions

A decrease in the microchannel width reduces the heat transfer resistance and increases the consumed pumping power of the μHTS (see Fig. 4a) and b)). The influence of the microchannel dimensions on the net output power of the generator is plotted for different flow rates in Fig. 7. A reduction in channel width directly leads to an enhancement of the actual temperature gradient across the μTEG and therefore an increase in the μTEG's output power. However, considering the net μTEG output power, the simultaneous increase in required pumping power P_{PUMP} counteracts this positive effect. Therefore, at higher fluid flows where higher pumping powers are needed (blue line), P_{PUMP} outweighs the reduced R_{HTS} for small microchannel widths, and larger channel widths yield better net power results. With decreasing flow rates the optimal channel width shifts towards smaller microchannel dimensions. At $\Delta T = 30$K, a fluid flow of 0.04 l/min and a channel width of 50 μm results in the maximal net output power. Considering the decreasing relative influence of the pumping power for increasing
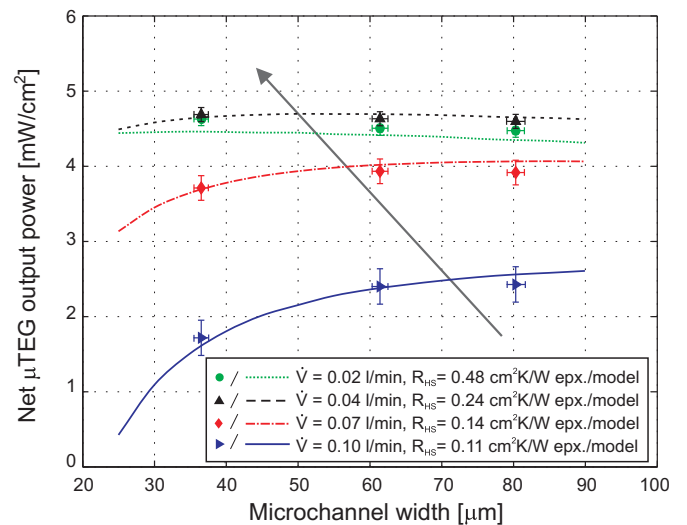

Fig. 6. Net output power measured for μTEGs with different ZT values (dashed lines with markers) and computed for a μTEG with $ZT = 1$ (solid line) as a function of the applied ΔT at a fluid flow rate of 0.07 l/min and w_{ch} = 35 μm.

Fig. 7. Measured (markers) and computed (lines) net output power of the μHTS/μTEG system as a function of the microchannel width and the applied fluid flow rate measured at a ΔT of 30K.

temperature differences ΔT applied, the impact of a reduced R_{HTS} will be more pronounced. According to simulations, at an applied temperature gradient of 90K, the maximal net power output is reached with a channel width of 35 μm, at a volumetric flow rate of 0.06 l/min. Therefore, knowing the standard operating conditions of the system, a custom microchannel design can be applied to achieve an optimal output performance.

3.2.3. Influence of μTEG thermal resistance

As shown in Fig. 5a), the influence of the varying heat transfer resistances, i.e. varying fluid flow, on the μTEG output power was small. This can be attributed to the fact that the thermal resistance of the μTEG $R_{TEG} = 5.1$ cm^{2}K/W) is significantly larger than the variation in the heat transfer resistance of the μHTS ($R_{HTS} = 0.11-0.48$ cm^{2}K/ W). To investigate the influence of a smaller difference in thermal resistance, the μTEG thickness was reduced in two steps. The measurement results and corresponding simulations are summarized in Fig. 8. The Seebeck voltage decreases with decreasing μTEG thickness and reduced flow rates (Fig. 8a)). This is a direct consequence of the reduced temperature gradient across the generator. The Seebeck voltage of a generator can be expressed in a simplified model (Joule heating and Peltier effects are neglected) [28]:

$$V_{Seebeck} = S\Delta T_{TEG} = S\frac{R_{TEG}}{R_{TEG} + R_{Con}}\Delta T \qquad (1)$$

where S is the Seebeck coefficient of the μTEG, ΔT_{TEG} is the temperature gradient at the generator surface and ΔT is the external thermal gradient. R_{Con} is defined as the sum of all thermal contact resistances, including the heat transfer resistance of the μHTS R_{HTS} and the interface resistances $R_{Interface}$ at both sides of the TEG (see Fig. 3). Each $R_{Interface}$ is estimated to be approximately 0.22 cm^{2}K/W, resulting in a total contact resistance R_{Con} between 0.55 cm^{2}K/W (0.1 l/min) and 0.92 cm^{2}K/W (0.02 l/min).

At μTEG thicknesses below 50 μm, the slope of the Seebeck voltage is very steep, since the μTEG thermal resistance is smaller than the total contact resistance ($R_{TEG} < R_{Con}$). Therefore, a small increase in the μTEG thickness results in a relative large increase in ΔT_{TEG}. With increasing thicknesses ($R_{TEG} > R_{Con}$), the curve becomes progressively flat due to the reduced influence of the μTEG

thickness on ΔT_{TEG}. At the same time, the influence of varying R_{HTS} becomes smaller with increasing μTEG thickness, which is indicated by the smaller spreading of the Seebeck voltage measurements for different fluid flows. This effect is more pronounced for the μTEG output power (Fig. 8b)), where the Seebeck voltage is squared (see equation in Fig. 8b) inset). The μTEG output power also increases with increasing μTEG thickness, it reaches a maximum and decreases again. In the first section, the power increase is again attributed to the increase of ΔT_{TEG}. At the maximum point, the thermal resistances of μTEG and contacts are approximately matched [12]. However, considering the Joule heating and Peltier cooling losses, there is a shift of the optimal point to larger μTEG thicknesses [28]. On the right side of the maxima, the negative influence of the increased electrical resistance of the generator dominates over the increase in the Seebeck voltage. With increased fluid flows applied, i.e. reduced R_{HTS}, the point of maximal output power shifts towards higher values and smaller μTEG thicknesses. A reduced heat transfer resistance results in higher ΔT_{TEG} and smaller μTEG thicknesses to achieve thermally matched resistances.

For each temperature operating range of the system, an optimal μTEG thickness can be defined to maximize the power output. For applications with lower ΔT available, where smaller fluid flows can be applied to reach the maximum net output power (see Fig. 8b)), the optimal μTEG thickness is around 90 μm. With increasing external temperature gradient and therefore increasing required fluid flows for optimal power exploitation, the μTEG thickness can be reduced even further. The presented optimal μTEG thicknesses are specific values for the μTEG used in this study. Changes in thermal and electrical properties of the generator will result in a shift of the maximal power points to different μTEG thicknesses. Small thicknesses enabled by the very low heat transfer resistance μHTS are of particular interest for energy harvesting from waste heat recovery. For example in industrial heat exchange systems, where high heat fluxes are required to sustain the necessary heat dissipation, a low thermal resistance of the generator is favorable. Additionally, a reduced μTEG thickness brings the advantages of smaller material and fabrication costs, as well reductions in system size and weight.

Another important aspect related to low heat transfer resistances is the relevance of the thermal properties of the thermoelectric material. The thermal resistance of a generator depends
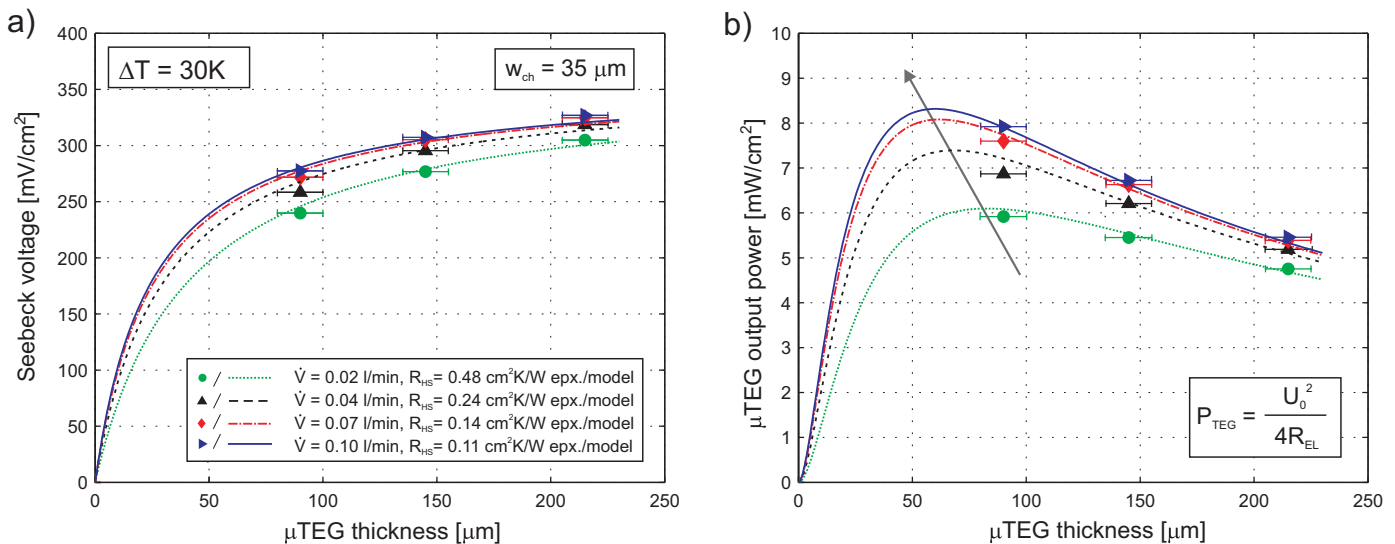

Fig. 8. Measured (markers) and computed (lines) (a) Seebeck voltage and (b) output power of the μHTS/μTEG system as a function of the μTEG thickness at an applied ΔT of 30K and a $w_{ch} = 35$ μm. The μTEG thermal resistances are R_{TEG} (90 μm) = 2.1 cm^{2}K/W, R_{TEG} (145 μm) = 3.4 cm^{2}K/W and R_{TEG} (215 μm) = 5.1 cm^{2}K/W. The total contact resistance R_{Con} lies between 0.55 cm^{2}K/W (0.1 l/min) − 0.92 cm^{2}K/W (0.02 l/min).
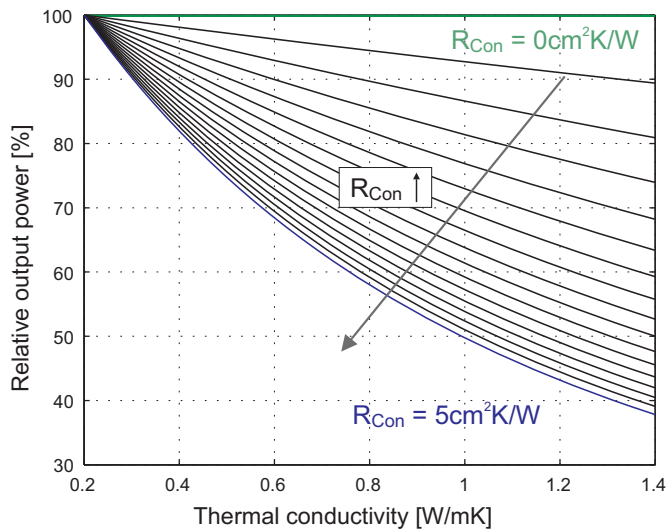
Fig. 9. Computed relative μTEG output power with respect to the thermal conductivity of the thermoelectric material λ and the thermal contact resistance R_{Con} (0–5 cm²K/Wm, in steps of 0.3 cm²K), referring to the value of $\lambda = 0.2$ W/mK. A μTEG thickness of 215 μm, ΔT of 30K, a thermal conductivity of the passive material of 0.3 W/mK, and parameters from Table 2 were used.

not only on the thickness, but also on the thermal conductivity of the active (and passive) material. When working with very small thermal contact resistances, the importance of low thermal conductivities is reduced. In Fig. 9 the relative μTEG output power is plotted versus the thermal conductivity λ of the thermoelectric material, for different thermal contact resistances R_{Con}. The relative power is normalized to a μTEG output power value potentially achieved with a very low thermal conductivity of $\lambda = 0.2$ W/mK (e.g. of a superlattice structure [8]). The relative influence of an increase in λ decreases with reduced R_{Con}. In the ideal case of $R_{Con} \rightarrow 0$, the output power becomes a function of only the Seebeck coefficient S, the electrical resistance R_{El} and the externally applied ΔT (see Formula 1 and inset in Fig. 8b)). Therefore, when working with very low heat transfer resistances, the material optimization efforts should shift from the optimization of the figure of merit $ZT = \alpha^2 \sigma T / \lambda$ to the enhancement of the power factor $P = \alpha^2 \sigma$. This would in particular refer to nanostructured composites [29,30] and superlattice structures [8], where an improvement of ZT is mainly achieved by the reduction of λ. This conclusion is in agreement with Narducci [31], who also emphasized the much higher relevance of the power factors over the ZT value, especially for high heat flux applications.

4. Conclusions

The proposed system integration of μTEGs with a low power consuming μHTS was characterized with respect to the generated net output power. The small heat transfer resistances enabled much higher effective temperature gradients across the μTEGs and led to a significant enhancement of the produced output power. The presented μHTS achieved heat transfer resistances between 0.17 and 0.88 cm²K/W at corresponding low pumping powers of 6.8 – 0.06 mW/cm².

Due to the coupled influence of μHTS/μTEG system parameters and boundary conditions, its net output performance can be optimized for different operating conditions by the applied fluid flow rate and by the careful design of the microchannels. A trade-off must be made between a low heat transfer resistance, i.e. a high effective temperature gradient, and the consumed pumping power. At smaller operating temperature differences, the impact of the

pumping power outweighs the reduced R_{HTS} and thus smaller flows and wider channels lead to higher net powers. With a larger temperature gradient applied, the influence of the consumed pumping power decreases and the optimal flow rate increases, whereas the optimal microchannel width decreases.

A system net output power of 126.3 ± 1.5 mW/cm² was measured with a module ZT of 0.1 at the applied temperature difference of 95K and a fluid flow rate of 0.07 l/min. It was shown that with the achieved thermal coupling, the μTEG thickness could be further reduced to 60–90 μm in order maximize the output power under thermally matched resistances. This brings several advantages with respect to fabrication and cost and makes the system suitable for high heat flux waste heat recovery applications. Moreover, the reduced relevance of the thermal conductivity in the thermoelectric material with decreasing contact resistances was highlighted. The discussed advantages and achieved performance demonstrated the potential for future up-scaling and further system extension into compact multi-layer heat exchangers for industrial applications.

References

[1] Anatychuk LI, Rozver YY, Velichuk DD. Thermoelectric generator for a stationary diesel plant. J Electron Mater 2011;40:1206–8.
[2] Crane DT, LaGrandeur JW, Harris F, Bell LE. Performance results of a high-power-density thermoelectric generator: beyond the couple. J Electron Mater 2009;38:1375–81.
[3] Jaensch D. Thermoelectric goes automotive. 2nd ed. Expert Verlag; 2011.
[4] Rowe DM. Applications of nuclear-powered thermoelectric generators in space. Appl Energ 1991;40:241–71.
[5] Bennett GL, Hemler RJ, Schock A. Space nuclear power: an overview. J Propul Power 1996;12:901–10.
[6] Lamp TR, Donovan BD. Unattended power sources for remote, harsh environments. In: 29th intersociety energy conversion engineering conference 1994. p. 688–93. Pts 1–4.
[7] Hunt TK, Sievers RK, Patania AC. Small AMTEC systems as battery substitutes. In Space technology and applications international forum, Pts 1 and 2 2000;vol. 504. p. 1356–60.
[8] Venkatasubramanian R, Siivola E, Colpitts T, O'Quinn B. Thin-film thermoelectric devices with high room-temperature figures of merit. Nature 2001;413:597–602.
[9] Harman TC, Walsh MP, Laforge BE, Turner GW. Nanostructured thermoelectric materials. J Electron Mater 2005;34:L19–22.
[10] Hsu KF, Loo S, Guo F, Chen W, Dyck JS, Uher C, et al. Cubic AgPbmSbTe2+m: bulk thermoelectric materials with high figure of merit. Science 2004;303: 818–21.
[11] Glatz W, Schwyter E, Durrer L, Hierold C. Bi₂Te₃-based flexible micro thermoelectric generator with optimized design. J Microelectromech S 2009;18: 763–72.
[12] Stevens JW. Optimal design of small ΔT thermoelectric generation systems. Energ Convers Manage 2001;42:709–20.
[13] Wojtas N, Schwyter E, Glatz W, Kühne S, Escher W, Hierold C. Power enhancement of micro thermoelectric generators by microfluidic heat transfer packaging. Sensor Actuat A: Phys 2012;188:389–95.
[14] Tsuyoshi A, Matsuura K. A trial manufacture of a thermoelectric generator powered by high-temperature heat transfer medium oil. Electr Eng Jpn 2002;141:36–44.
[15] Niu X, Yu JL, Wang SZ. Experimental study on low-temperature waste heat thermoelectric generator. J Power Sources 2009;188:621–6.
[16] Crane D, Bell L, LaGrandeur J. Progress report on vehicular waste heat recovery using a cylindrical thermoelectric generator. In: Jaensch D, editor. Thermoelectrics goes automotive. Expert Verlag; 2011. p. 83–91.
[17] Tuckerman DB, Pease RFW. High-performance heat sinking for VlSI. Electron Device Lett 1981;2:126–9.
[18] Agostini B, Fabbri M, Park JE, Wojtan L, Thome JR, Michel B. State of the art of high heat flux cooling technologies. Heat Transfer Eng 2007;28:258–81.
[19] Rezania A, Rosendahl LA. Evaluating thermoelectric power generation device performance using a rectangular microchannel heat sink. J Electron Mater 2011;40:481–8.

[20] Escher W, Poulikakos D, Brunschwiler T, Michel B. Experimental investigation of an ultrathin manifold microchannel heat sink for liquid-cooled chips. J Heat Trans T ASME 2010;132.

[21] Colgan EG, Furman B, Gaynes M, LaBianca N, Magerlein JH, Polastre R, et al. High performance and subambient silicon microchannel cooling. J Heat Trans T ASME 2007;129:1046–51.

[22] Boteler L, Jankowski N, Geil B, McCluskey P. A Micromachined manifold microchannel cooler. In: . Proceedings of the ASME IMECE2009 2010;vol. 5. p. 61–8.

[23] Schwyter ES, Helbling T, Glatz W, Hierold C. Fully automated measurement setup for non-destructive characterization of thermoelectric materials near room temperature. Rev Sci Instrum 2012;83.

[24] Strasser M, Aigner R, Lauterbach C, Sturm TF, Franosch M, Wachutka G. Micromachined CMOS thermoelectric generators as on-chip power supply. Sensor Actuat A-Phys 2004;114:362–70.

[25] UKAS. U.K.A. Service, editor. The expression of uncertainty and confidence in measurement. United Kingdom Accreditation Service; 2007.

[26] Escher W, Poulikakos D, Michel B. A novel high performance, ultra thin heat sink for electronics. Int J Heat Fluid Fl 2010;31:586–98.

[27] Strasser M, Aigner R, Franosch M, Wachutka G. Miniaturized thermoelectric generators based on poly-Si and poly-SiGe surface micromachining. Sensor Actuat A-Phys 2002;97-8:535–42.

[28] Glatz W, Muntwyler S, Hierold C. Optimization and fabrication of thick flexible polymer based micro thermoelectric generator. Sensor Actuat A-Phys 2006;132:337–45.

[29] Ma Y, Hao Q, Poudel B, Lan YC, Yu B, Wang DZ, et al. Enhanced thermoelectric figure-of-merit in p-type nanostructured bismuth antimony tellurium alloys made from elemental chunks. Nano Lett 2008;8:2580–4.

[30] Kim W, Zide J, Gossard A, Klenov D, Stemmer S, Shakouri A, et al. Thermal conductivity reduction and thermoelectric figure of merit increase by embedding nanoparticles in crystalline semiconductors. Phys Rev Lett 2006;96.

[31] Narducci D. Do we really need high thermoelectric figures of merit? A critical appraisal to the power conversion efficiency of thermoelectric materials. Appl Phys Lett 2011;99.